Published in final edited form as:
Cell Calcium. 2010 November ; 48(5): 275–287. doi:10.1016/j.ceca.2010.09.007.

A helix-breaking mutation in the epithelial Ca^{2+} channel TRPV5 leads to reduced Ca^{2+}-dependent inactivation

Kyu Pil Lee[a,1], **Anil V. Nair**[a,1], **Christian Grimm**[b,c,d,1], **Femke van Zeeland**[a], **Stefan Heller**[b,c,d], **René J.M. Bindels**[a], and **Joost G.J. Hoenderop**[a,*]

Joost G.J. Hoenderop: J.Hoenderop@fysiol.umcn.nl

[a]Department of Physiology, Radboud University Nijmegen Medical Centre, The Netherlands [b]Department of Otolaryngology, Stanford University School of Medicine, Stanford, CA 94305, USA [c]Department of Head and Neck Surgery, Stanford University School of Medicine, Stanford, CA 94305, USA [d]Department of Molecular and Cellular Physiology, Stanford University School of Medicine, Stanford, CA 94305, USA

Abstract

TRPV5, a member of transient receptor potential (TRP) superfamily of ion channels, plays a crucial role in epithelial calcium transport in the kidney. This channel has a high selectivity for Ca^{2+} and is tightly regulated by intracellular Ca^{2+} concentrations. Recently it was shown that the molecular basis of deafness in varitint-waddler mouse is the result of hair cell death caused by the constitutive activity of transient receptor potential mucolipin 3 (TRPML3) channel carrying a helix breaking mutation, A419P, at the intracellular proximity of the fifth transmembrane domain (TM5). This mutation significantly elevates intracellular Ca^{2+} concentration and causes rapid cell death. Here we show that substituting the equivalent location in TRPV5, the M490, to proline significantly modulates Ca^{2+}-dependent inactivation of TRPV5. The single channel conductance, time constant of inactivation (τ) and half maximal inhibition constant (IC_{50}) of TRPV5(M490P) were increased compared to TRPV5(WT). Moreover TRPV5(M490P) showed lower Ca^{2+} permeability. Out of different point mutations created to characterize the importance of M490 in Ca^{2+}-dependent inactivation, only TRPV5(M490P)-expressing cells showed apoptosis and extremely altered Ca^{2+}-dependent inactivation. In conclusion, the TRPV5 channel is susceptible for helix breaking mutations and the proximal intracellular region of TM5 of this channel plays an important role in Ca^{2+}-dependent inactivation.

1. Introduction

The superfamily of TRP channels plays a major role in sensory transduction, ionic homeostasis and cell differentiation [1–4]. The TRP genes encode for subunit with six transmembranespanning domains that assemble into tetrameric cation channels. Mammalian TRPs are classified into six subfamilies based on sequence homology: TRPCs (Canonical), TRPVs (Vanilloid), TRPMs (Melastatin), TRPAs (Ankyrin), TRPPs (Polycystin), and TRPMLs (Mucolipin) [1,3,5,6]. Besides the general understanding that TRP channels conduct cations, they have diverse structural and functional features [1–3]. For example, relative Ca^{2+} permeabilities (P_{Ca2+}/P_{Na+}) range from low (TRPM4 and TRPM5) to high (TRPV5 and TRPV6) [7,8]. Additionally, TRPV5 and TRPV6 are strongly regulated by the

*Corresponding author at: Department of Physiology, Radboud University Nijmegen Medical Centre, 286 Physiology, P.O. Box 9101, 6500 HB Nijmegen, The Netherlands. Tel.: +31 24 3610580; fax: +31 24 3616413.
[1]These authors contributed equally to this work.

changes in intracellular Ca^{2+} ($[Ca^{2+}]_i$). A critical functional regulatory mechanism of these two channels involves inhibitory feedback by $[Ca^{2+}]_i$ [9].

Physiologically, TRPV5 and TRPV6 play a key role in Ca^{2+} reabsorption in the kidney and intestine [10–12]. A wide variety of factors regulate the activity of TRPV5 such as the klotho protein, tissue kallikrein, pH, Ca^{2+}, and other associated proteins [8]. Studies have indicated that different sites in TRPV5 are involved in Ca^{2+}-dependent channel regulation. The aspartic acid residue at position 542 of the pore region between the 5th and 6th transmembrane-spanning domains (TM5 and TM6) is essential for the Ca^{2+} selectivity [13]. Nilius and coworkersdemonstrated that two intracellular domains, A650-C653 and G701-F730, in the carboxyl-terminus are responsible for Ca^{2+}-dependent inactivation of TRPV5 [14]. Moreover, they also reported that the intracellular loop between TM2 and TM3, particularly L409, V411, and T412, determines the initial rapid inactivation kinetics of TRPV6 [15]. However, the structural basis of the molecular mechanism underlying the Ca^{2+}-dependent inactivation of these channels remains unresolved.

The TRP channels, which play important roles as cellular sensors, are involved in a multitude of Ca^{2+}-dependent cell functions. This implies that failure in proper channel function can lead to complex pathophysiological conditions. Channelopathies in which mutant TRP genes directly cause cellular dysfunction are glomerulosclerosis (TRPC6), mucolipidosis type IV (TRPML1), hypomagnesemia with secondary hypocalcaemia (TRPM6), and polycystic kidney disease (TRPP1/TRPP2) [16]. A recent addition to this list was dysfunction in TRPML3 causing varitint-waddler (*Va*) phenotype [17–19]. The *Va* phenotype is caused by a mutation, A419P, at the proximal pore region of TM5. This mutation leads to cell death by robustly increasing $[Ca^{2+}]_i$ [20,21]. Introduction of a proline (or glycine) into a rigid helical structure generally results in a kink, hinge or swivel in the structure [22–24], which might lead to functional abnormality. In some naturally occurring situations similar to shaker-type potassium channels, presence of proline in a helical structure is necessary for normal channel gating as the movement of one part of the helix opens the gate [24–26]. In the case of TRPML3 it has been postulated that the mutation causes constitutive activity, thus increasing $[Ca^{2+}]_i$ leading to cell death [20]. Grimm et al. [20] explored via sequence alignment whether other TRP channels display similar propensity. They demonstrated that HEK293 cells expressing TRPML1(V432P), TRPML2(A396P), TRPV5(M490P) or TRPV6(M497P) exhibited elevated $[Ca^{2+}]_i$ with respect to their wild-type isoforms [20]. The mechanism by which $[Ca^{2+}]_i$ is elevated in the case of TRPV5/6 channels may or may not reflect that of TRPML channels, since the channels function differently when analyzed in identical conditions. However, the helix breaking mutations in TRPV5/6 were speculated to play a role in Ca^{2+}-dependent inactivation either by directly locking the channel in a constitutively active mode, or indirectly, by reducing the effectiveness of inactivation.

In this study, we functionally characterized the helix breaking mutation in TRPV5 based on previous finding by Grimm et al. [20] that TRPV5(M490P) has an increased $[Ca^{2+}]_i$ compared to TRPV5(WT). To this end, different point mutations (M490P, M490L, M490G, M490D and M490C) were made and channel properties were studied using a combined electrophysiological-biochemical approach. Except TRPV5(M490L) all other point mutations had altered the single channel conductivity, $[Ca^{2+}]_i$ sensitivity and Ca^{2+}-dependent inactivation properties of the channel to some extend. Among these point mutations, TRPV5(M490P) had altered the channel characteristics severely.

2. Experimental procedures

2.1. DNA constructs and cell culture

TRPV5 was sub-cloned in the pcDNA3.1-YFP expression vector via XhoI restriction sites. Different M490 mutants (M490P, M490L, M490G, M490D and M490C) of TRPV5 were generated by *in vitro* mutagenesis (Quick-Change Site-Directed Mutagenesis kit, Stratagene, La Jolla, CA, USA). All constructs were verified by sequence analysis. HEK293 cells were maintained in Dulbecco's modified Eagle's medium supplemented with 10% (v/v) fetal bovine serum. Cells were transiently transfected using Lipofectamine 2000 according to manufacturer's (Invitrogen Life Technologies, Breda, The Netherlands) protocol and used 16 h after transfection for immunoblotting, and patch-clamp experiments. In the cell rescue experiments, we applied 2–5 mM of EDTA in the culture medium, however, we obtained the best results with 2 mM EDTA. At this EDTA concentration, incubation of the cells for 24 h did not result in cell death or altered cell morphology.

2.2. Cell surface biotinylation

HEK293 cells were seeded on fibronectin-coated plates. After 5 h the cells were transfected with mTRPV5-YFP pcDNA3.1 or mTRPV5-YFP M490P pcDNA3.1. EDTA was added in the medium and cells were incubated for 18 h at 37°C. Subsequently, cells were biotinylated, lysed and precipitated from the cell lysates with neutravidin beads (Pierce, Ettenleur, The Netherlands) as described previously [27]. Biotinylation was performed in the cold room (4°C) and cells were homogenized in 0.5 ml lysis buffer (1% (v/v) NP-40, 150 mM NaCl, 5 mM EDTA, 1mM PMSF, 10 mg/ml leupeptin, 10 mg/ml pepstatin, 50 mM Tris/HCl, pH 7.5). For equal loading, protein concentration in total lysates was measured by using the BCA protein assay kit (Thermo Scientific, Rockford, IL, USA), according to the manufacturer's manual.

2.3. Immunoblotting

Cells were washed with phosphate-buffered saline solution (PBS, pH 7.2), and lysed in Laemmli/Dithiothreitol solution. Total protein fractions were separated on 8% (w/v) SDS-PAGE gels and blotted to polyvinylidene difluoride-nitrocelulose membranes (Immobilon-P, Millipore, Bedford, MA). Blots were incubated with rabbit anti-GFP (1:4000, Sigma) or with mouse anti β-actin (1:10,000, Sigma) overnight at 4°C. After successive washings, secondary antibodies, either peroxidase-conjugated goat anti-rabbit antibody (1:10,000, Sigma) or peroxidase-conjugated sheep antimouse antibody (1:10,000, Jackson) was added to the immunoblots and incubated at room temperature for 1 h. Immunoreactive protein was detected using the enhanced chemiluminescence method as described by the manufacturer (Amersham, Buckinghamshire, UK).

2.4. Annexin V and confocal analysis

HEK293 cells were directly grown on coverslips and transfected with plasmid DNAs encoding wild-type or mutant channels fused carboxy-terminally with enhanced green fluorescent protein (eGFP) or yellow fluorescent protein (YFP). After 10, 15, 20, and 24/25 h of transfection, the cells were washed with PBS and then exposed to Cy5-conjugated annexin V binding buffer (BD Biosciences, San Jose, CA), incubated at room temperature for 5 min in the dark, and analyzed using Laser Scanning Microscopy (LSM 510, Zeiss, Germany or FV1000, Olympus, USA). Quantification of the number of transfected HEK293 cells that bound Cy5-conjugated annexin V, was performed in three independent experiments for each time point.

2.5. Electrophysiology

Patch clamp experiments were performed as described previously [7] in the tight seal whole-cell or cell attached configuration at room temperature using an EPC-9 patch-clamp amplifier controlled by the Pulse software (HEKA Elektronik, Lambrecht, Germany). Cells were kept in nominal divalent free solution to prevent calcium overload. For whole cell patch clamp, patch pipettes had resistance between 2 and 4 MΩ after filling with the standard intracellular solution. Cells were held at +20 mV, and voltage ramps of 450 ms ranging from −100 to +100 mV were applied to measure current–voltage (*I/V*) relations. Ca^{2+} currents were measured for 2.5 s at −100 mV stepping from a holding potential of +70 mV. Cell capacitance and access resistance were continuously monitored using the automatic capacitance compensation of the Pulse software. Current densities were obtained by normalizing the current amplitude to the cell membrane capacitance. To measure the permeability of monovalent cations with respect to Na^+, cells were held at 0 mV and voltage ramp of 200 ms ranging from −100 to +100 mV at an interval of 3 s was applied. Cells were exposed to Na^+ free ($NMDG^+$) solution in between two monovalent cationic solutions. In the case of relative Ca^{2+} permeability experiments, the ramp protocol consisted of linear voltage ramps for 60 ms ranging from −100 to +100 mV stepped from +70 mV at an interval of 100 ms was applied. For cell attached single channel recording, pipette resistance was between 7 and 10 MΩ. Channel conductance was measured using step protocol ranging from −100 mV to +100 mV in 20 mV increments and every step was lasting for 1 s. The single channel recordings were performed at a sampling rate of 10 kHz and were filtered at 1 kHz.

2.6. Solutions

For whole cell patch clamp measurements, nominal divalent free solution contained (mM): 150 NaCl, 6 CsCl, 10 Glucose and 10 HEPES/NaOH, pH 7.4. To measure Na^+ current density, 50 μM EDTA was added to the nominal divalent free solution to chelate divalent cations (divalent free, DVF). 150 mM NaCl was replaced with an equimolar amount of N-methyl-D-glucamine-Cl (NMDG-Cl) to inhibit monovalent cation currents. 10 mM $CaCl_2$ was added in NMDG-Cl solution to measure Ca^{2+} current. Osmotic differences were adjusted by adding the respective concentrations of mannitol to the Ca^{2+}-free solutions. The standard intracellular solution contained (mM): 100 Cs-aspartate, 20 CsCl, 1 $MgCl_2$, 10 BAPTA, 4 Na_2-ATP, 10 HEPES/CsOH, pH 7.2. To adjust the $[Ca^{2+}]_i$ to various concentrations, the appropriate amount of $CaCl_2$ was added in the presence of 10 mM BAPTA, as determined by the CaBuf program (ftp://ftp.cc.kuleuven.ac.be/pub/droog-mans/cabuf.zip).

For monovalent cation relative permeability experiments, the standard extracellular solution contained (mM): 150 $NMDG^+$, 2 HEDTA, 10 HEPES, pH7.4/HCl (Na^+ free solution). Other monovalent ion solutions contained 150 mM of Na^+, Li^+, K^+, Rb^+, or Cs^+ instead of $NMDG^+$ (pH7.4/NMDG-OH). Osmotic differences were adjusted by adding respective amount of mannitol. For relative Ca^{2+} permeability experiments, the solution was prepared by isosmotically replacing $NMDG^+$ with 10 mM Ca^{2+} in the Na^+ free solution.

For single channel measurements, cells were perfused with the following solution to set the membrane potential at 0 mV (mM): 140 KCl, 5 EDTA, 5 EGTA, 1 $MgCl_2$, 10 Glucose and 10 HEPES/KOH, pH 7.2 and the pipette solution contained (mM): 140 NaCl, 10 EGTA and 10 HEPES/NaOH, pH 7.4.

2.7. Data analysis

Whole cell patch clamp data were analyzed using Igor pro software (Wavemetrics, Lake, Oswege, USA). The permeability ratios of monovalent cations (X^+) to Na^+ were calculated

from the shift in reversal potential (V_{rev}) upon replacement of extracellular solution with respective cations using the equation

$$\frac{P_{X^+}}{P_{Na^+}} = \exp\left(\frac{\Delta v_{rev} F}{RT}\right) \quad (1)$$

The Δv_{rev} was determined relative to Na^+ from the same cells to avoid effect of leak current. The permeability ratio of Ca^{2+} to Na^+ was determined by using the following equation

$$\frac{P_{Ca^{2+}}}{P_{Na+}} = \left(1+\exp\left(\frac{v_{rev}F}{RT}\right)\right) \times \frac{([Na^+]_i + \alpha[Cs^+]_i)\exp(v_{rev}F/RT) - [Na^+]_e - [Cs^+]_e}{4[Ca^{2+}]_e} \quad (2)$$

where α is P_{Cs+}/P_{Na+}. All potentials were corrected for liquid junction potential using JPCalcW software [28]. Single channel data analysis was performed using TAC software (Bruxton, Seattle, USA). Data are expressed as mean ± SEM. Statistical significance was determined by one-way ANOVA when there were three or more groups, and in the case of overall significance Bonferroni's multiple comparison test was used. $P < 0.05$ was considered significant in both cases.

3. Results

3.1. TM5 of TRPMLs and TRPV5/TRPV6 have significant sequence identity

TRP channels share a common tetrameric membrane topology. They comprise six TM spanning regions and a short hydrophobic pore-forming region in every subunit (Fig. 1B). Recently Grimm et al. [20] deduced the molecular mechanism underlying the *Va* phenotype and attributed this to a helix-break caused by the A419P mutation in TM5 oftheTRPML3 channel. They further showed that TRPV5 and TRPV6 are also susceptible for helix-breaking mutations in TM5 along with the TRPML family. Amino acid sequence alignment of the TM5 domains of TRPV5 and TRPML3 indicated a significant (24.7%) sequence identity. Fig.1A shows sequence alignment of human (Hs) and murine (Mm) TRPML3 and TRPV5/TRPV6. TRPV5 has M490 (Mm) and M497 (Hs) as equivalent positions to that of A419 (Hs and Mm) in TRPML3.

3.2. Proline substitution at M490 results in cell death

To investigate the functional consequences of this mutation on TM5, we decided to use murine TRPV5, hereafter referred to as TRPV5(WT) unless otherwise mentioned. By site directed mutagenesis we replaced M490 with proline (TRPV5(M490P)). Wild-type and mutant channels were expressed in HEK293 cells and analyzed with the whole-cell patch clamp technique. TRPV5(WT) showed the characteristic strong inwardly rectifying current [29]. Current traces were elicited by using a ramp voltage (−100 mV to +100 mV, holding +20 mV) in the presence of DVF (refer to Section 2.5) solution (Fig. 2A). The data were routinely normalized to cell capacitance. Averaged Na^+ current density of TRPV5(WT) at −80 mV was 1515 ± 183 pA/pF ($n = 21$). TRPV5(M490P) expressing cells showed a significantly decreased Na^+ current amplitude (627 ± 84 pA/pF, $n = 7$, $p < 0.05$) (Fig. 2A,B). Interestingly, the majority of HEK293 cells expressing TRPV5(M490P) had an altered cell morphology (round and/or floating). For Na^+ current measurement we picked cells that were still attached to the coverslip with a comparable morphology to that of TRPV5(WT) expressing cells. The reduced Na^+ current density measured from these cells was probably due to low protein expression compared to that of TRPV5(WT) expressing cells.

TRPV5 channels are the gatekeepers of active Ca^{2+} reabsorption in kidney epithelial cells [9,11]. As a functional regulatory mechanism they undergo Ca^{2+}-induced inhibition by binding Ca^{2+} from the intracellular side. Measuring the inward current carried by Ca^{2+} and the Ca^{2+}-dependent inactivation characteristics gives important information about the normal properties of the channel. Unfortunately we were not able to measure the current carried by Ca^{2+} from TRPV5(M490P) expressing HEK293 cells because all the patches were lost upon exposure to 10 mM Ca^{2+} containing extracellular solution.

Next, we analyzed TRPV5 expression from mutant and wildtype expressing HEK293 cells using anti-GFP antibody. Although some TRPV5(M490P)-expressing cells were detectable by the YFP fusion marker, the overall expression of the mutant channel in the cultures was at the detection limit of immunoblot analysis (Fig. 2C).

In their seminal work, by using Ca^{2+} imaging technique, Grimm et al. showed that HEK293 cells expressing TRPV5(M490P) had higher basal Ca^{2+} level. Thus the altered morphology and reduced viability of the TRPV5(M490P)-expressing cells was an indication of disturbed $[Ca^{2+}]_i$ and metabolism of the cell. To investigate this, we probed TRPV5(WT) and TRPV5(M490P)-expressing HEK293 cells with annexin V-Cy5, an early apoptosis marker. We found that 10 h after transfection, nearly 40% of the TRPV5(M490P) expressing cells were annexin V positive. Within the next 10 h, the number of annexin positive cells increased to more than 75% (Fig. 2D and E). We hypothesize that massive increase in intracellular Ca^{2+} leads to a significant amount of apoptosis in cells expressing the mutant channel.

3.3. Chelating extracellular Ca^{2+} prevents cytotoxicity in TRPV5(M490P) expressing cells

To confirm that Ca^{2+} overload was cytotoxic in TRPV5(M490P) expressing cells, the extracellular Ca^{2+}($[Ca^{2+}]_e$) was chelated from the culture medium by adding EDTA, which should rescue the cells from dying. We also hypothesized that this strategy would enable us to functionally characterize the mutant. We added 2 mM EDTA to the HEK293 cells after transfecting with TRPV5(M490P). Fig. 3A shows cell membrane expression of TRPV5(WT) and TRPV5(M490P) protein with and without 2 mM EDTA treatment. Chelating extracellular Ca^{2+} prevented its overload and subsequent cell death in the cells expressing TRPV5(M490P) thus increased the amount of detectable protein in the plasma membrane fraction similar to that of TRPV5(WT) (Fig. 3A). The Na^+ current measured from the rescued mutant channel expressing cells showed *I/V* characteristics and current density similar to that of TRPV5(WT)-expressing HEK293 cells (Fig. 3B and C) (TRPV5(M490P), 512 ± 66 pA/pF, $n = 11$; TRPV5(M490P)+2 mM EDTA, 1549 ± 208 pA/pF, $n = 11$). The Na^+ current density measured from TRPV5(WT)-expressing cells treated with EDTA did not change significantly compared to that from non-treated TRPV5(WT)-expressing cells. (TRPV5(WT), 1509 ± 142 pA/pF, $n = 13$; TRPV5(WT) + 2 mM EDTA, 1661 ± 241 pA/pF, $n = 5$). The Ca^{2+} current measured in the presence of 10 mM $[Ca^{2+}]_e$ still showed a significantly lower current density measured from the peak at −100 mV (Fig. 3D and E) in the case of TRPV5(M490P) compared to TRPV5(WT) (TRPV5(WT), 802 ± 100 pA/pF, $n = 12$; TRPV5(M490P) + 2 mM EDTA, 486 ± 51 pA/pF, $n = 10$). Remarkably, Fig. 3D shows that Ca^{2+}-induced inactivation of TRPV5(M490P)-expressing cells was significantly slower compared to that of TRPV5(WT).

3.4. Plasma membrane calcium ATPase type 2 suppresses apoptosis mediated by TRPV5(M490P)

To pinpoint whether the cytotoxic effect of TRPV5(M490P) is Ca^{2+}-mediated, the Ca^{2+} extrusion pump, plasma membrane Ca^{2+} ATPase type 2 (PMCA2) was coexpressed with TRPV5 [21,30]. We probed TRPV5(WT) and TRPV5(M490P)-expressing HEK293 cells

with annexin V-Cy5 for 10 and 24 h after transfection. TRPV5(WT)-expressing cells treated with 2 mM EDTA did not show asignificant change in morphology or channel expression (Fig. 4A and B). However, coexpression of PMCA2 with TRPV5(WT) reduced the transfection efficiency. After 10 hrs of transfection < 5% of cells were found annexin V positive in the control condition, whereas no annexin V positive cells were observed in the group treated with EDTA or cotransfected with PMCA2 (10 h). The cells treated with EDTA for 24 h displayed reduced amount of annexin V positive cells in the control condition. On the other hand TRPV5(WT) and PMCA2 cotransfected cells in the control were not found to be annexin V positive (Fig. 4C). In the case of TRPV5(M490P) mutants, after 10 h, the transfected cells were rounded up or floating and showed a strong staining for annexin V. Interestingly, cells treated with 2 mM EDTA or cotransfected with PMCA2 were found negative for annexin V staining (Fig. 4D–F). 24 h after transfection, EDTA-treated cells expressing TRPV5(M490P) mutant channels (Fig. 4E) showed significantly less positive staining for annexin V compared to TRPV5(M490P) control cells (Fig. 4D and E). The PMCA2 cotransfected cells depicted less than 2% positive staining after 24 h of transfection (Fig. 4F). Previously, it has been shown that the carboxy-terminus of TRPV5(WT) is involved in Ca^{2+}-dependent inactivation of the channel and some of the carboxy-terminal truncated mutant-expressing cells demonstrated an altered morphology and low channel expression [14,31]. Subsequent experiments indicated that the transfection efficiency of TRPV5(698X) was increased and the cell morphology was rescued by the addition of 2 mM of EDTA to the medium after transfection (Fig. 4G and H).

3.5. TRPV5(M490P) shows altered Ca^{2+} permeability

In order to classify the TRPV5(WT) and TRPV5(M490P) pore properties, we determined the relative monovalent cation and relative Ca^{2+} permeability with respect to Na^+. To measure the maximal current for each monovalent cation, the bath solution was alternately switched between $NMDG^+$ solution and solutions containing the single permeant cation (Fig. 5A–D). The permeability ratios for Li^+, K^+, Rb^+ and Cs^+ were calculated by using the shift in V_{rev} upon application of different permeant cation species using equation 1 (Fig. 5K). Of note, some cells expressing both wild-type and mutant channels showed outward currents while exposed to extracellular solution containing NaCl. When the outward current was more than 20% of the inward current (~15% of the cells), cells were omitted from analysis. In order to determine the Ca^{2+} permeability with respect to Na^+, bath solution containing 150 mM of NaCl was switched to solutions containing $NMDG^+$ and 10 mM of Ca^{2+} (Fig. 5E and F). The reversal potential measurement showed that TRPV5(WT) reached to a peak of 41.1 ± 5.3 mV compared to 25.0 ± 5.3 mV in the mutant. The V_{rev} measurements after 20 s of Ca^{2+} application displayed a minimum of −2.6 ± 3.5 mV in the TRPV5(WT) compared to a minimal of 13.4 ± 1.5 mV in the mutant. The relative permeability ratio of Ca^{2+} to Na^+ showed a mean value of 113.6 ± 47.2 in the TRPV5(WT) compared to 24.5 ± 6.0 in the TRPV5(M490P) mutant (Fig. 5L). On the contrary after 20 s of Ca^{2+} application, the relative Ca^{2+} permeability reduced to 4.3 ± 1.3 in the TRPV5(WT) compared to 9.1 ± 0.9 in the mutant. The ratio of maximum permeability to the minimum permeability is depicted in Fig. 5M. The reversal potentials and permeability ratios are summarized in Table 1. Our results indicated a perturbed pore architecture in TRPV5(M490P) compared to the wild-type channel.

3.6. Effect of mutating M490 to amino acids with different chemical properties

Proline has a distinctive cyclic side chain which locks its dihedral angle at approximately −75°. This gives proline an exceptional conformational rigidity and can act as a secondary structure disruptor. When substituted in an otherwise rigid α-helical conformation, proline disrupts the structure with a swivel, kink or hinge [23,32,33]. Glycine (G) is also known to perturb a rigid helical structure [22,33], because of the very small (only a Hydrogen atom)

and flexible side chain. Helix propensity or frequency of certain amino acids to be found in an alpha helix varies considerably from alanine (very high) to proline (very low) [34]. Negatively charged and highly hydrophilic aspartate (D) is considered to have very low helix propensity next to that of glycine. Cysteine (C) follows the list after D [34], whereas the charged amino acid leucine (L) has very high propensity to be in an alpha helix [34]. We mutated M490 to different amino acids (P, L, C, D and G) to determine whether disrupting the helical structure with lesser severity will lead to more Ca^{2+} induced inactivation compared to TRPV5(M490P).

Fig. 6A shows the protein expression pattern of different amino acid substitutions at M490. TRPV5(M490C) displays lower expression that is due to a lower efficiency of transfection, judged by the lesser percentage of fluorescent cells seen per transfection when compared to other transfected mutants. Fig. 6B–D depicts the *I/V* curves and current density histograms of different mutants. The *I/V* curves were elicited by ramp protocol in the presence of DVF solution and normalized to cell capacitance. Current responses corresponding to −80 mV from the *I/V* curve were used to plot histograms. TRPV5(M490P) and TRPV5(M490D) had significantly smaller Na^+ current density than that of TRPV5(WT), 1509 ± 142 pA/pF, n = 13; TRPV5(M490P), 512 ± 66 pA/pF, n = 11; TRPV5(M490L), 1533 ± 135 pA/pF, n = 20; TRPV5(M490C), 1099 ± 41 pA/pF, n = 15; TRPV5(M490G); 1231 ± 135 pA/pF, n = 14; TRPV5(M490D), 864 ± 27 pA/pF, n = 15).

As expected, except for TRPV5(M490L) all other mutant channels had different Ca^{2+}-induced inactivation characteristics and Ca^{2+} current densities (Fig. 6E). To measure Ca^{2+} current from TRPV5(M490P) mutant expressing cells, they were supplemented with 2 mM EDTA in the culture media (+EDTA in Fig. 6F–H). The current traces obtained by applying 10 mM extracellular Ca^{2+} to TRPV5(WT) and different mutant expressing cells were fitted to an equation for single exponential decay and the corresponding fitted curves are shown as a grey overlay in Fig. 6E. One of the clear and remarkable differences between TRPV5(WT) and TRPV5(M490P) was the slow inactivation. Fig. 6F showed the peak Ca^{2+} current (black) obtained at −100 mV and the residual current after 2.5 s (white). The residual current, or the percentage of channels contributing to the Ca^{2+} current after 2.5 s in the case of TRPV5(M490P), was substantially higher compared to all other mutants and wildtype, suggesting a highly disturbed Ca^{2+}-induced inactivation of this mutant (Fig. 4G). Fig. 6H shows the inhibition time constant τ, obtained from the exponential fit displayed in Fig. 6E. All mutants except for TRPV5(M490L) showed significantly different τs from wild-type; TRPV5(M490P) displayed the highest difference. These results showed that TRPV5(M490P) had severely altered Ca^{2+}-induced inactivation properties.

3.7. Proline substitution at M490 changes $[Ca^{2+}]_i$-dependent inactivation of TRPV5(WT) channels

Fig. 6E–H suggests that the intrinsic Ca^{2+}-dependent auto-regulation of TRPV5(WT) channel was disrupted in the TRPV5(M490P) mutant. To investigate the change in Ca^{2+} concentration dependency on inactivation, we measured whole cell Na^+ current in the presence of extracellular DVF solution by varying intracellular calcium concentrations. The appropriate intracellular free Ca^{2+} concentration was calculated by using Calbuf software (see Section 2 for details) and accordingly the solution was prepared. As $[Ca^{2+}]_i$ increased, Na^+ currents decreased in a dose dependent manner. In the case of TRPV5(WT), 172 ± 18 nM of Ca^{2+} inhibited 50% (IC_{50}) of current measured in the absence of Ca^{2+} (Fig. 7A). The TRPV5(M490P) isoform also showed decreased Na^+ currents as intracellular Ca^{2+} concentration increased, but with a significantly higher IC_{50} than that of TRPV5(WT) (3008 ± 154 nM). Likewise, the TRPV5(M490C) mutant showed a shift of the dose-response curve to the right (412 ± 61 nM, $p < 0.001$). Other mutants did not alter the Ca^{2+} dependency of inactivation (TRPV5(M490L), 78 ± 26 nM; TRPV5(M490G), 77 ± 14 nM;

TRPV5(M490D), 49 ± 2 nM) (Fig. 7B). We conclude that the intracellular Ca^{2+} accumulation of TRPV5(M490P) mutant, and subsequent cell death is caused by severely decreased Ca^{2+}-dependent inactivation in combination with an increased time constant of inactivation.

3.8. Met490 to proline mutation increases the single channel conductance

Substituting different amino acids of distinct chemical features might also have altered the respective single channel conductance. To investigate this, we performed cell-attached single channel measurements. This experiments were conducted with Na^{+}-containing pipette solution. Cells were kept in a solution containing 5 mM EDTA and 5 mM EGTA to curb increase of $[Ca^{2+}]_i$. Fig. 8A depicts a representative single channel current trace obtained from TRPV5(WT) expressing HEK293 cells in response to voltage stepping from −100 mV to 0 mV in 20 mV increments. We determined a single channel conductance of 57.0 ± 1.2 pS in the case of TRPV5(WT) (n = 8). TRPV5(M490P) showed an increased single channel conductance of 75.9 ± 3.6 pS (n = 10) compared to TRPV5(WT) (Fig. 8A and B). Other mutant channels except for TRPV5(M490G) showed comparable single channel conductances to that of TRPV5(WT) (TRV5(M490L),66.8 ± 6.1 pS, n=5, TRPV5(M490C), 64.2 ± 7.7 pS, n = 5) (Fig. 8C and D). In the case of TRPV5(M490G), measurements from four different cells displayed a reduced single channel conductance of 40.3 ± 5.5 pS. We were not able to generate single channel data from TRPV5(M490D)in the cell attached mode, probably due to very small single channel current amplitudes.

4. Discussion

TRPV5 is the gatekeeper of transcellular Ca^{2+} transport in the kidney epithelial cells, thus plays a remarkable role in the overall Ca^{2+} homeostasis in the body [8,10,35]. It is a cation-selective channel with high permeability for Ca^{2+} but can also conduct monovalent cations in the absence of extracellular divalent cations [7,29,36]. A crucial functional regulatory feature of this channel is the feedback inhibition mechanism by intracellular Ca^{2+} [9]. Our present study shows the important role played by the intracellular region of TM5 in this inhibitory mechanism. This study is based on previous findings that a mutation at A419 in TRML3 causes the varitint-waddler phenotype [18,20,37]. After detailed sequence analysis and further site directed mutagenesis Grimm et al. [20] concluded that TRPV5 and TRPV6 share the susceptibility for helix breaking mutations with TRPML channels. In the present study, we elucidated the functional differences caused by this mutation at a homologous position, M490, of TRPV5. Both TRPML3 [20] and TRPV5 data show that mutant channel-expressing cells undergo a considerable amount of apoptosis (~40%) already 10 h after transfection. We can not pinpoint that TRPV5(M490P) and TRPML3(A419P) expressing cells undergo apoptosis by the same mechanism since under similar physiological conditions TRPV5 is constitutively active and TRPML3 is closed. However, we show that apoptosis of TRPV5(M490P) expressing cells also occurs as a consequence of Ca^{2+} overload. Current notion in the case of TRPML3 is that it becomes constitutively active by helix breaking mutations in TM5. Nevertheless, helix breaking mutations indeed caused a Ca^{2+} overload in both mutant channel expressing cells, which suggests a similar structure/function relationship in these channels.

Amino acids vary in their helix propensity owing to different chemical and physical properties [34]. Due to proline's unique structural rigidity its introduction to an otherwise noncompliant helical structure often causes swivels, hinges or kinks [23,32–34,38]. Interestingly, the evolutionarily conserved PXP motif in the S6 (TM6) segment of shaker family K^{+} channels creates a flexible “hinge” that allows movement of the lower S6 segment during “normal” channel gating and opening [24]. Mutations also alter single channel properties and pore behavior of an ion channel. Here, we show that substituting

M490 to different amino acids alters the Ca^{2+} permeability, reversal potential and single channel properties of TRPV5(WT) channel. In the present study, introducing a point mutation to the TM5 of TRPV5(WT) helped in understanding the important role played by this segment in Ca^{2+}-dependent feedback inhibition mechanism and its selectivity, which is likely to be shared by the close family member TRPV6, and probably also by all three TRPML members.

4.1. Consequence of proline substitution in TM5 of murine TRPV5 on the relative Ca^{2+}-permeability

Ca^{2+} channels rely on four glutamate or aspartate residues for ion selectivity, whose carboxyl side chains likely face the pore lumen to interact with passing Ca^{2+} ions [39,40]. This structure is thought to be flexible, tightly binding a single Ca^{2+} ion (high affinity site) in order to block Na^+ flux [39]. The slow ion flux nature of high affinity binding is avoided in a multi-ion pore environment by intrapore ion-ion interaction. In this situation, one high-affinity ion elutes the other and so selectivity with high flux is allowed [39]. To classify the selectivity and pore ionic strength, we determined the relative monovalent and Ca^{2+} permeability of TRPV5(WT) and TRPV5(M490P) (Fig. 5) channels. The relative monovalent permeability ratios of the wild-type and mutant channel were not altered (Fig. 5K) except for the large cation $NMDG^+$. Even though the P_{X^+}/P_{Na^+} was similar for the permeant cations, the reversal potentials were altered (refer to Table 1). This is due to the fact that ΔE_{rev} values were comparable for both TRPV5(WT) and TRPV5(M490P). In the case of wild-type, the permeability ratios of Li^+, K^+, Rb^+, Cs^+ and $NMDG^+$ relative to Na^+ were 0.80 ± 0.01, 0.57 ± 0.01, 0.50 ± 0.03, 0.47 ± 0.03 and 0.07 ± 0.01, respectively. This sequence ($Na^+ > Li^+ > K^+ > Rb^+ > Cs^+$) corresponds to Eisenman sequence X [41], indicating the second highest ionic field strength binding sequence. The mutant TRPV5(M490P) also displayed the same selectivity sequence with permeability ratios, 0.77 ± 0.01, 0.53 ± 0.02, 0.47 ± 0.02, 0.45 ± 0.02 and 0.16 ± 0.03 for Li^+, K^+, Rb^+, Cs^+ and $NMDG^+$, respectively. Although there is no difference in the selectivity sequence between TRPV5(WT) and TRPV5(M490P), the smaller E_{rev} values of monovalent cations (Table 1) and higher permeability for $NMDG^+$ indicated an expanded pore in the case of TRPV5(M490P). These observations were consistent with the finding by Yeh et al. [42] that increasing the extracellular pH (pH_e) from 6.0 to 7.4 increased the pore diameter from 6.3 to 7.5 Å, but the selectivity sequence remained the same (Eisenman X). However, increasing the pH_e to 9 increased the pore diameter to 11.8 Å, changing the selectivity sequence from Eisenman X to IV or V [42], which shows a weak pore field ionic strength. Another proof for alteration of the pore architecture comes from the relative Ca^{2+} to Na^+ permeability measurements. TRPV5(WT) has ~100 times higher Ca^{2+} selectivity compared to Na^+, but in the case of TRPV5(M490P) it has reduced to ~20 times (Fig. 5L&M). These data clearly indicate an increase in pore size, thus reducing the affinity for Ca^{2+} binding. Decreasing the field strength in the Ca^{2+} binding site might enlarge the competition between Na^+ and Ca^{2+} in the pore. Moreover, the intrapore ion-ion interactions also might alter. This is reminiscent with the finding that the Na^+ peak current is comparable between TRPV5(WT) and TRPV5(M490P) whereas the Ca^{2+} peak current is significantly smaller (Fig. 4B-E). Recently, it has been shown that the *Va* phenotype causing mutation, TRPML3(A419P), can stably expand the pore. Furthermore, it also altered the pore field ionic strength and changed the selectivity sequence from Eisenman XI to X [43].

4.2. The effect of TRPV5(M490P) on Ca^{2+}-induced feedback inhibition mechanism

So far, it has been reported that the molecular mechanism of Ca^{2+}-induced feedback inhibition in TRPV5 involves two carboxyl terminus regions, G701–F730 and A650–C653. In the case of the closely related and highly homologous family member TRPV6, it has been shown that three amino acids (L409, V411 and T412) situated at the loop between TM2 and

TM3 are responsible for the fast inactivation. Moreover TRPV6 contains Ca^{2+}-dependent CaM binding motif in the carboxyl terminus, which acts as a negative feedback system [14, 15]. The helix breaking mutation, TRPV5(M490P) at the TM5 domain modulates the Ca^{2+}-induced feedback inhibition mechanism severely. Compared to TRPV5(WT), TRPV5(M490P) had a >15 times higher IC_{50} of intracellular Ca^{2+} (172 ± 18 *versus* 3008 ± 154 nM, respectively). Keeping in mind that the physiological level of $[Ca^{2+}]_i$ is in the nM range, one can imagine the profound effect of this mutation on cytotoxicity when expressed heterologously. In addition, the time constant of inactivation (τ) also increased considerably in this mutant compared to TRPV5(WT). Though other amino acid substitutions (G, C and D) at this location have changed the IC_{50} and τ values compared to TRPV5(WT), the effect induced by proline substitution stands out. Our single channel analysis shows an increased channel conductance in the case of the P substitution and a decreased conductance in the case of the G substitution, suggesting that perturbation of the proximal region of TM5 alters the pore.

In conclusion, in the context with what is known about Ca^{2+}-dependent inactivation, the feedback inactivation mechanism does not appear only to reside in the carboxyl region, but also in the intracellular proximity of TM5. Our finding raises several questions with respect to these regions. For instance, as seen in the case of TRPV6, does the loop between TM5 and TM6 play a role in inactivation? Does the helix-breaking mutation itself impede the binding of Ca^{2+}? Or, Ca^{2+} might still be able to interact with its binding pocket, but the energy transferred to the pore region is altered, because TM5 can not successfully translate the molecular rearrangement and force TM6 and pore region to close the (inactivation) gate. Another question to answer is, what is the role of the carboxylic terminal domain in this whole process? Future work is necessary to shed more light on these aspects. From our current results, we can conclude that the helix breaking mutation TRPV5(M490P) disrupts the Ca^{2+} selectivity, pore size and normal Ca^{2+}-dependent feedback inhibition mechanism. We further conclude that the proximal intracellular region of TM5 plays a crucial role in the functionally critical Ca^{2+}-dependent inactivation mechanism of TRPV5 channels.

Acknowledgments

The authors have been supported by grants of the Netherlands Organization for Scientific Research [grant number ZonMw 9120.6110], a EURYI award from the European Science Foundation, and the Dutch Kidney Foundation [grant number C05.2134].

References

1. Venkatachalam K, Montell C. TRP channels. Annu Rev Biochem. 2007; 76:387–417. [PubMed: 17579562]
2. Clapham DE. TRP channels as cellular sensors. Nature. 2003; 426:517–524. [PubMed: 14654832]
3. Ramsey IS, Delling M, Clapham DE. An introduction to TRP channels. Annu Rev Physiol. 2006; 68:619–647. [PubMed: 16460286]
4. Damann N, Voets T, Nilius B. TRPs in our senses. Curr Biol. 2008; 18:R880–889. [PubMed: 18812089]
5. Clapham DE, Montell C, Schultz G, Julius D. International Union of Pharmacology. XLIII. Compendium of voltage-gated ion channels: transient receptor potential channels. Pharmacol Rev. 2003; 55:591–596. [PubMed: 14657417]
6. Montell C, Birnbaumer L, Flockerzi V, et al. A unified nomenclature for the superfamily of TRP cation channels. Mol Cell. 2002; 9:229–231. [PubMed: 11864597]
7. Nilius B, Vennekens R, Prenen J, Hoenderop JG, Bindels RJ, Droogmans G. Whole-cell and single channel monovalent cation currents through the novel rabbit epithelial Ca^{2+} channel ECaC. J Physiol. 2000; 527(Pt. 2):239–248. [PubMed: 10970426]

8. Hoenderop JG, Nilius B, Bindels RJ. Calcium absorption across epithelia. Physiol Rev. 2005; 85:373–422. [PubMed: 15618484]
9. Nilius B, Prenen J, Vennekens R, Hoenderop JG, Bindels RJ, Droogmans G. Modulation of the epithelial calcium channel, ECaC, by intracellular Ca^{2+} Cell Calcium. 2001; 29:417–428. [PubMed: 11352507]
10. Hoenderop JG, Bindels RJ. Calciotropic and magnesiotropic TRP channels. Physiology (Bethesda). 2008; 23:32–40. [PubMed: 18268363]
11. Hoenderop JG, Nilius B, Bindels RJ. Epithelial calcium channels: from identification to function and regulation. Pflugers Arch. 2003; 446:304–308. [PubMed: 12684797]
12. Hoenderop JG, Bindels RJ. Epithelial Ca^{2+} and Mg^{2+} channels in health and disease. J Am Soc Nephrol. 2005; 16:15–26. [PubMed: 15574510]
13. Nilius B, Vennekens R, Prenen J, Hoenderop JG, Droogmans G, Bindels RJ. The single pore residue Asp542 determines Ca^{2+} permeation and Mg^{2+} block of the epithelial Ca^{2+} channel. J Biol Chem. 2001; 276:1020–1025. [PubMed: 11035011]
14. Nilius B, Weidema F, Prenen J, et al. The carboxyl terminus of the epithelial Ca^{2+} channel ECaC1 is involved in Ca^{2+}-dependent inactivation. Pflugers Arch. 2003; 445:584–588. [PubMed: 12634930]
15. Nilius B, Prenen J, Hoenderop JG, et al. Fast and slow inactivation kinetics of the Ca^{2+} channels ECaC1 and ECaC2 (TRPV5 and TRPV6). Role of the intracellular loop located between transmembrane segments 2 and 3. J Biol Chem. 2002; 277:30852–30858. [PubMed: 12077127]
16. Nilius B. TRP channels in disease. Biochim Biophys Acta. 2007; 1772:805–812. [PubMed: 17368864]
17. Kim HJ, Li Q, Tjon-Kon-Sang S, So I, Kiselyov K, Muallem S. Gain-of-function mutation in TRPML3 causes the mouse Varitint-Waddler phenotype. J Biol Chem. 2007; 282:36138–36142. [PubMed: 17962195]
18. Xu H, Delling M, Li L, Dong X, Clapham DE. Activating mutation in a mucolipin transient receptor potential channel leads to melanocyte loss in varitint-waddler mice. Proc Natl Acad Sci USA. 2007; 104:18321–18326. [PubMed: 17989217]
19. Cuajungco MP, Samie MA. The varitint-waddler mouse phenotypes and the TRPML3 ion channel mutation: cause and consequence. Pflugers Arch. 2008; 457:463–473. [PubMed: 18504603]
20. Grimm C, Cuajungco MP, van Aken AF, et al. A helix-breaking mutation in TRPML3 leads to constitutive activity underlying deafness in the varitint-waddler mouse. Proc Natl Acad Sci USA. 2007; 104:19583–19588. [PubMed: 18048323]
21. Grimm C, Jors S, Heller S. Life and death of sensory hair cells expressing constitutively active TRPML3. J Biol Chem. 2009; 284:13823–13831. [PubMed: 19299509]
22. Cuajungco MP, Samie MA. The varitint-waddler mouse phenotypes and the TRPML3 ion channel mutation: cause and consequence. Pflugers Arch. 2008
23. Cordes FS, Bright JN, Sansom MS. Proline-induced distortions of transmembrane helices. J Mol Biol. 2002; 323:951–960. [PubMed: 12417206]
24. Labro AJ, Raes AL, Bellens I, Ottschytsch N, Snyders DJ. Gating of shakertype channels requires the flexibility of S6 caused by prolines. J Biol Chem. 2003; 278:50724–50731. [PubMed: 13679372]
25. Seebohm G, Strutz-Seebohm N, Ureche ON, et al. Differential roles of S6 domain hinges in the gating of KCNQ potassium channels. Biophys J. 2006; 90:2235–2244. [PubMed: 16326905]
26. Sukhareva M, Hackos DH, Swartz KJ. Constitutive activation of the Shaker Kv channel. J Gen Physiol. 2003; 122:541–556. [PubMed: 14557403]
27. Chang Q, Hoefs S, van der Kemp AW, Topala CN, Bindels RJ, Hoenderop JG. The beta-glucuronidase klotho hydrolyzes and activates the TRPV5 channel. Science. 2005; 310:490–493. [PubMed: 16239475]
28. Barry PH. JPCalc, a software package for calculating liquid junction potential corrections in patch-clamp, intracellular, epithelial and bilayer measurements and for correcting junction potential measurements. J Neurosci Methods. 1994; 51:107–116. [PubMed: 8189746]
29. Vennekens R, Hoenderop JG, Prenen J, et al. Permeation and gating properties of the novel epithelial Ca^{2+} channel. J Biol Chem. 2000; 275:3963–3969. [PubMed: 10660551]

30. Zeevi DA, Lev S, Frumkin A, Minke B, Bach G. Heteromultimeric TRPML channel assemblies play a crucial role in the regulation of cell viability models and starvation-induced autophagy. J Cell Sci. 2010; 123:3112–3124. [PubMed: 20736310]

31. de Groot T, Verkaart S, Xi Q, Bindels RJ, Hoenderop JG. The identification of histidine 712 as a critical residue for constitutive TRPV5 internalization. J Biol Chem. 2010; 285:28481–28487. [PubMed: 20628046]

32. Sansom MS, Weinstein H. Hinges, swivels and switches: the role of prolines in signalling via transmembrane alpha-helices. Trends Pharmacol Sci. 2000; 21:445–451. [PubMed: 11121576]

33. Bright JN, Sansom MSP. The flexing/twirling helix: exploring the flexibility about molecular hinges formed by proline and glycine motifs in transmembrane helices. J Phys Chem B. 2003; 107:627–636.

34. Pace CN, Scholtz JM. A helix propensity scale based on experimental studies of peptides and proteins. Biophys J. 1998; 75:422–427. [PubMed: 9649402]

35. Hoenderop JG, Muller D, Suzuki M, van Os CH, Bindels RJ. Epithelial calcium channel: gate-keeper of active calcium reabsorption. Curr Opin Nephrol Hypertens. 2000; 9:335–340. [PubMed: 10926168]

36. Vennekens R, Prenen J, Hoenderop JG, Bindels RJ, Droogmans G, Nilius B. Pore properties and ionic block of the rabbit epithelial calcium channel expressed in HEK 293 cells. J Physiol. 2001; 530:183–191. [PubMed: 11208967]

37. Nagata K, Zheng L, Madathany T, Castiglioni AJ, Bartles JR, Garcia-Anoveros J. The varitint-waddler (Va) deafness mutation in TRPML3 generates constitutive, inward rectifying currents and causes cell degeneration. Proc Natl Acad Sci USA. 2008; 105:353–358. [PubMed: 18162548]

38. Barlow DJ, Thornton JM. Helix geometry in proteins. J Mol Biol. 1988; 201:601–619. [PubMed: 3418712]

39. Sather WA, McCleskey EW. Permeation and selectivity in calcium channels. Annu Rev Physiol. 2003; 65:133–159. [PubMed: 12471162]

40. Gillespie D. Energetics of divalent selectivity in a calcium channel: the ryanodine receptor case study. Biophys J. 2008; 94:1169–1184. [PubMed: 17951303]

41. Eisenman G. Cation selective glass electrodes and their mode of operation. Biophys J. 1962; 2:259–323. [PubMed: 13889686]

42. Yeh BI, Kim YK, Jabbar W, Huang CL. Conformational changes of pore helix coupled to gating of TRPV5 by protons. EMBO J. 2005; 24:3224–3234. [PubMed: 16121193]

43. Kim HJ, Yamaguchi S, Li Q, So I, Muallem S. Properties of the TRPML3 channel pore and its stable expansion by the Varitint-Waddler-causing mutation. J Biol Chem. 2010; 285:16513–16520. [PubMed: 20378547]

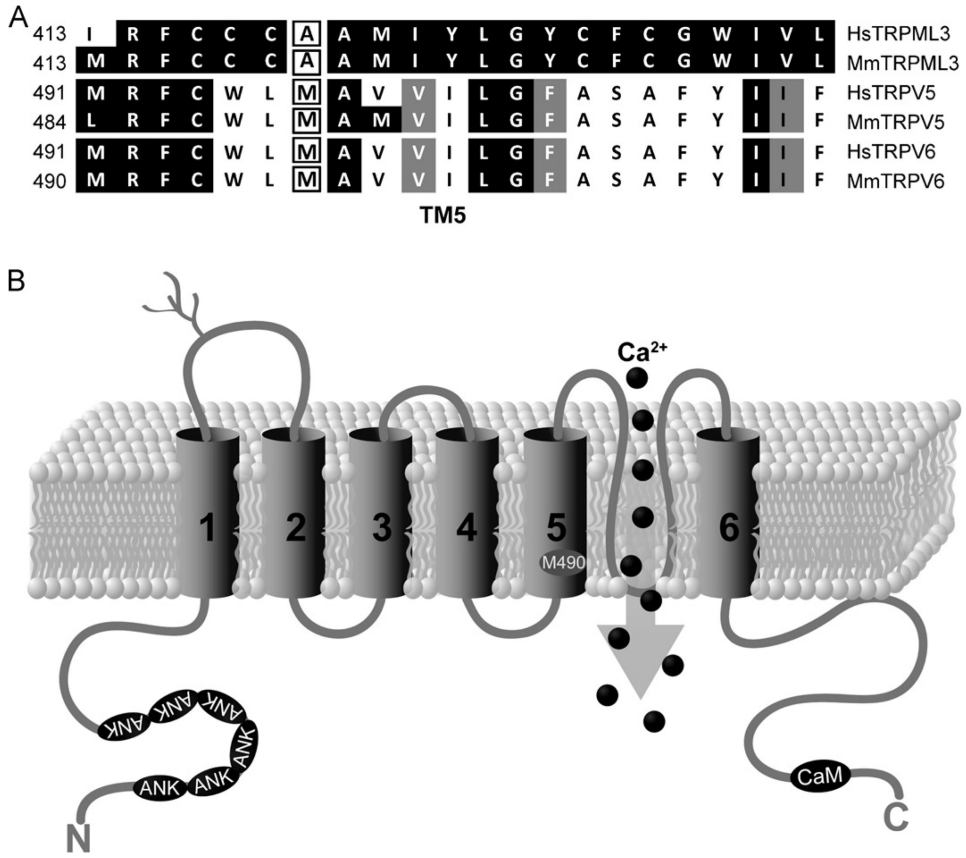

Fig. 1.

Sequence alignment of the 5th transmembrane domain of TRPML3, TRPV5 and TRPV6 channels. (A) Amino acid sequence comparison of TM5 of human (Hs) and Murine (Mm) TRPML3 with TRPV5 and TRPV6. (B) Schematic topology showing the putative position of TRPV5(M490) (shown as M490) in TM5. The six ankyrin repeats are depicted as ANK and the putative calmodulin-binding domain as CaM.

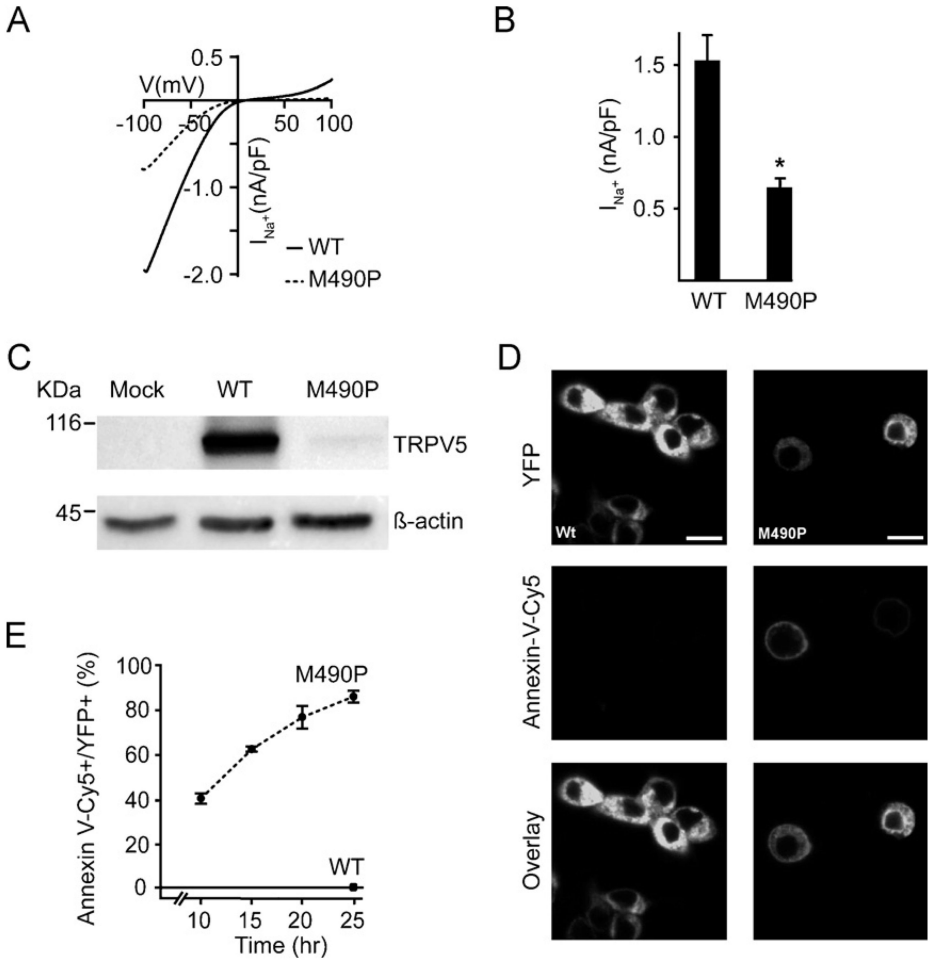

Fig. 2.

TRPV5(M490P), similar to TRPML3(A419P), shows altered whole cell current density compared to TRPV5(WT). (A and B) Na^+ current density of HEK293 cells expressing TRPV5(M490P) and TRPV5(WT) channels measured with divalent free (DVF) solution. Current–voltage relations (A) were elicited by ramp voltage from −100 mV to +100 mV and histogram (B) was plotted by taking current density corresponding to −80 mV holding potential. The substitution at M490 with a proline led to decreased Na^+ current density compared to TRPV5(WT). (C) Western blot analysis showing the protein expression of TRPV5(WT) and TRPV5(M490P). β-actin is taken as control for equal loading. The amount of TRPV5(M490P) mutant in the total lysate was beyond the detection limit of western blot technique used. (D) Annexin V, an apoptosis marker, binding to HEK293 cells expressing TRPV5(WT) and TRPV5(M490P). (E) Quantification of the number of transfected HEK293 cells that bound Cy5-conjugated annexin V. Shown are time points after transfection with TRPV5(WT) and TRPV5(M490P). The values are shown as mean± SEM. $*P < 0.05$, comparison with TRPV5(WT).

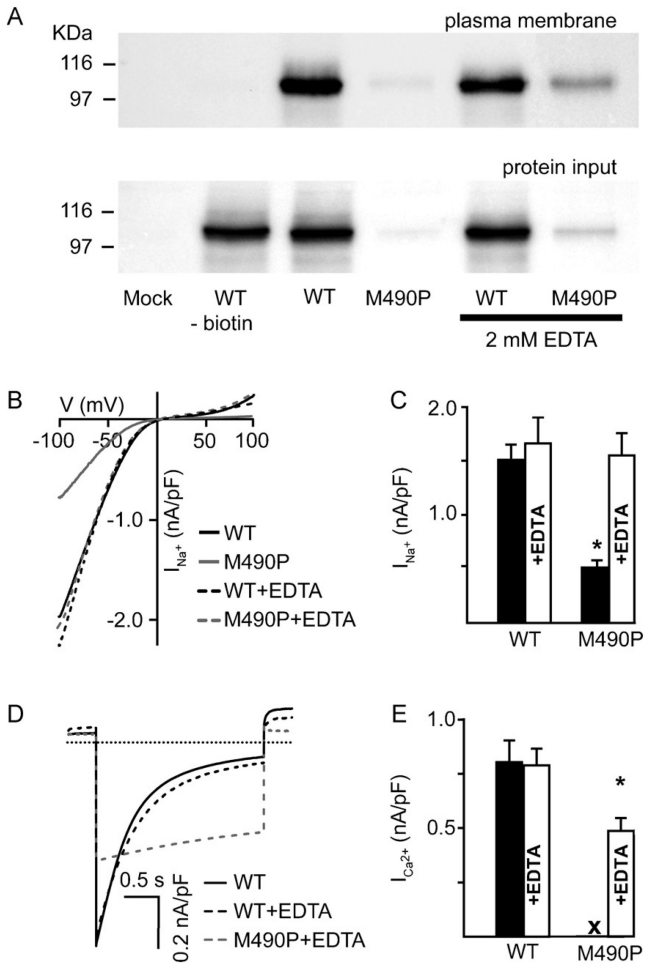

Fig.3.

Extracellular application of Ca^{2+} chelator EDTA rescues TRPV5(M490P) transfected HEK293 cells. (A) Effect of chelating $[Ca^{2+}]_e$ on detectable protein level of TRPV5(WT) and TRPV5(M490P). Cells transfected with TRPV5(WT) and TRPV5(M490P) were cultured for 16 h in normal DMEM culture media containing 10% (v/v) FCS or DMEM +10% (v/v) FCS supplemented with 2 mM EDTA. Cell surface biotinylation of this preparation shows an increase in the detectable TRPV5(M490P) protein level compared to non-treated mutant expressing cells. (B and C) Chelation of $[Ca^{2+}]_e$ in TRPV5(M490P) culture medium restores the sodium current density similar to that of TRPV5(WT). Addition of 2 mM EDTA in the culture media increased the sodium current of TRPV5(M490P) to the level of wild-type TRPV5. Chelation of $[Ca^{2+}]_e$ from the culture media of TRPV5(WT) expressing cells did not alter the Na^+ current density measured from these cells. (D and E) Ca^{2+} current measured from TRPV5(M490P) cells shows a decreased Ca^{2+} dependent inactivation. We were able to measure calcium current from TRPV5(M490P) expressing cells cultured in the presence of 5 mM EDTA. These cells showed a very slow Ca^{2+} dependent inactivation of current as shown in panel D. The dotted line in panel D indicates zero current level. The histogram in panel E shows that the Ca^{2+} current density obtained from the peak current measured at −100 mV is significantly lower in the case of TRPV5(M490P). The bars in (C) and (E) are also labeled +EDTA to indicate that the current was measured from the cells grown in the presence of EDTA. Histogram in C and E are shown as mean ± SEM. $*P < 0.05$, comparison with TRPV5(WT).

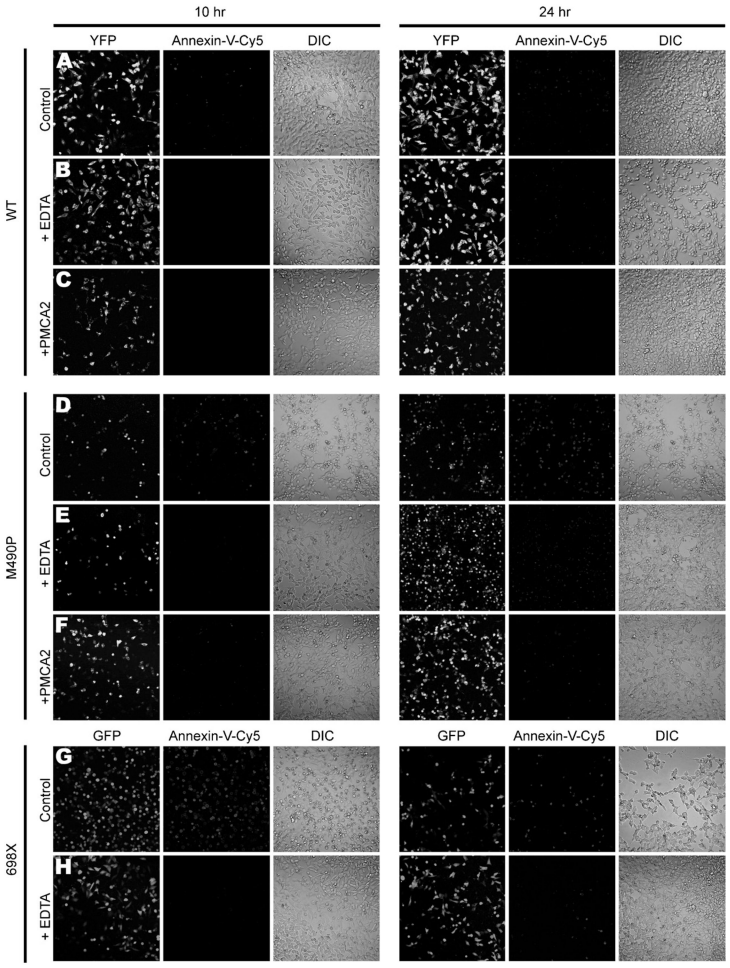

Fig. 4.

Coexpressing PMCA2 with TRPV5(M490P) rescues the cells from apoptosis. (A–C). Annexin V staining in TRPV5(WT) channels (control, control + 2 mM EDTA, cotransfection with PMCA2) expressing HEK293 cells. The first three panels in (A) indicates the confocal image of TRPV5(WT)-YFP, Annexin V and the DIC images respectively after 10 h of transfection. Panel 4–6 shows similar data but after 24 h of transfection. (B and C) The images of TRPV5(WT) treated with 2 mM EDTA and cotransfected with PMCA2, respectively, whereas the mutant channel TRPV5(M490P) is depicted in (D–F). (G and H) Similar experiments were performed with the truncated mutant 698X-GFP (control, control + 2 mM EDTA), at the indicated time points.

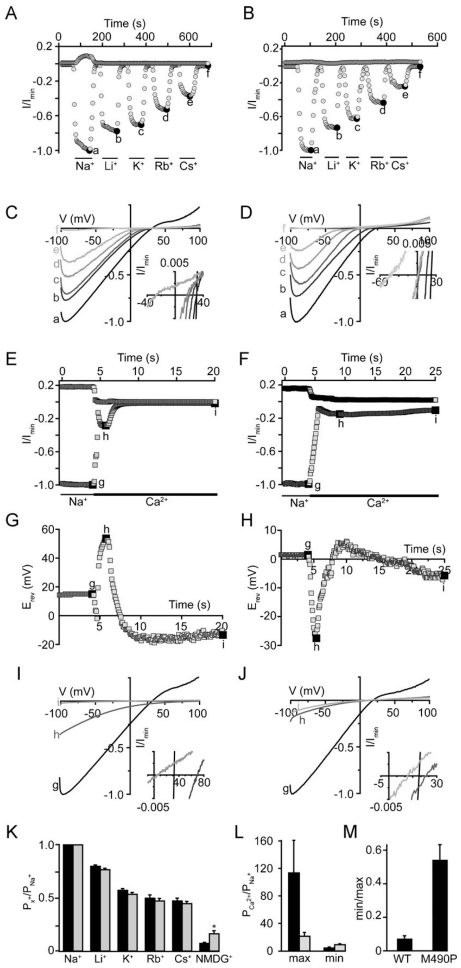

Fig. 5.

Permeation profiles of monovalent cations and Ca^{2+} for TRPV5(WT) and TRPV5(M490P). (A–D) Monovalent currents and *I/V* relations were measured in the presence of 150 mM of the indicated cations. (E and F), the relative Na^{+} to Ca^{2+} currents for TRPV5(WT) and TRPV5(M490P). (G and H) The corresponding reversal potential changes have been extracted from (E and F). (I and J) Shown are the *I/V* relations extracted corresponding to the time points indicated by the alphabets in E–H. The inset in C, D, I and J displays the *I/V* relation in an expanded scale to show the reversal potential. (K) Summary of the relative permeability for wild-typeTRPV5 (dark bars) and TRPV5(M490P) (grey bars). Data are the mean of 9–14 experiments. (L) Summary of Ca^{2+} to Na^{+} permeability ratios, measured at the peak (dark bars) and after inhibition by Ca^{2+} (grey bars). Results are the mean of 8–10 experiments. (M) The ratio of Ca^{2+} permeability values obtained from the E_{rev} of peak (h) and after the Ca^{2+}-induced inhibition (i) of TRPV5(WT) and TRPV5(M490P). Data are shown as mean ± SEM. $*P < 0.05$, comparison with TRPV5(WT).

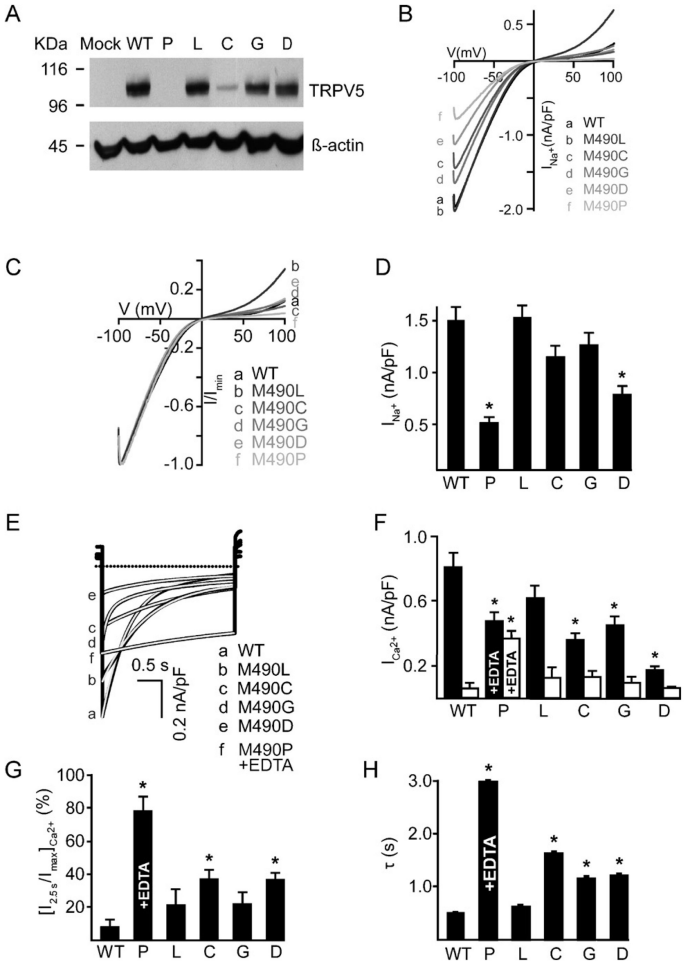

Fig. 6.

The effects of substitution of M490 to various amino acids on sodium and calcium current. (A) Western blot analysis showing the protein expression of TRPV5(WT), TRPV5(M490P), TRPV5(M490L), TRPV5(M490C), TRPV5(M490G) and TRPV5(M490D). To confirm equal input, 10% of total lysate was loaded and was probed against β-actin antibody. We could not detect the TRPV5(M490P) protein from the total cell lysate. The low intensity band corresponding to TRPV5(M490C) is due to the lower efficiency of transfection, judged by percentage of fluorescent cells in the total transfection well. (B–D) Sodium current density measured using DVF solution of mutants indicated. The M490 substitution to a proline or aspartic acid led to significantly decreased Na^+ current density compared to TRPV5(WT). (C) For better comparison *I/V* relations shown in (B) were normalized. (E) Ca^{2+} current traces obtained from mutant channels indicated. Except TRPV5(M490L), all other mutants showed significantly different Ca^{2+} current densities. The overlaid grey curves on the current traces indicate the curve fit to a single exponential decay equation. Except TRPV5(M490G), all other traces were very well fitted by a single exponential. TRPV5(M490G) was fitted by using an equation for double exponential and the faster component of 'τ' is shown in the panel H. The Ca^{2+} current trace in the case of TRPV5(M490P) was obtained from the cells which were grown in the presence of 2 mM EDTA after transfection. The dotted line indicates zero current level. (F) Histogram depicting the current density at the first time point of −100 mV step (I_{max}, black bars) and after 2.5 s ($I_{2.5s}$, white bars). Comparison of both black and white bars shows the extent of Ca^{2+} induced inhibition of channels after 2.5 s. (G) The percentage of initial peak Ca^{2+}

current persisted after 2.5 s. (H) Histogram showing the inhibition time constant τ obtained from the respective fits shown in panel E. Note that the mutant TRPV5(M490P) has longer time constant of inhibition and nearly 70% of current remained unaffected even after 2.5 s of 10 mM $[Ca^{2+}]_e$ application. The bars corresponding to TRPV5(M490P) in (F–H) are labeled +EDTA to indicate that the Ca^{2+} current was measured from the cells grown in the presence of EDTA. All Ca^{2+} currents were measured using a step protocol lasting 2.5 s, corresponding to −100 mV. In D and F–H values are shown as mean ± SEM. *P< 0.05, comparison with TRPV5(WT).

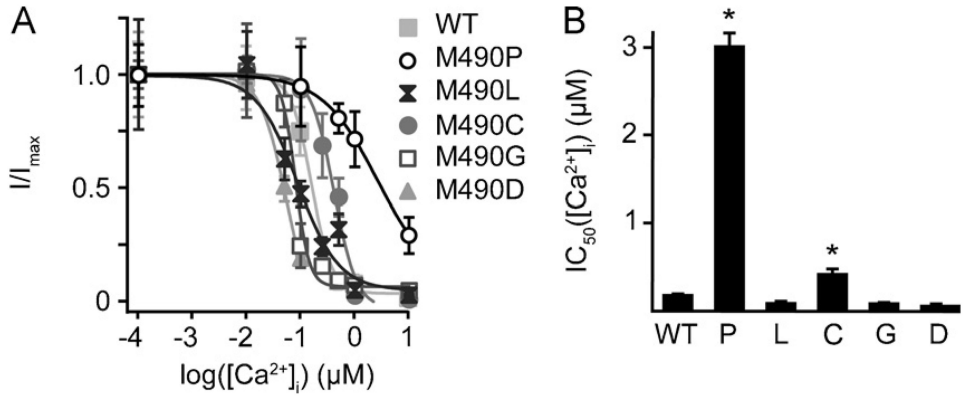

Fig. 7.

Proline substitution at M490 in TRPV5 led to lesser $[Ca^{2+}]_i$ sensitivity. (A) TRPV5(M490) shows reduced $[Ca^{2+}]_i$ sensitivity on DVF current. Dose–response analysis of $[Ca^{2+}]_i$ dependency on DVF current of TRPV5(WT) and respective mutants show that TRPV5(M490) has a very high IC_{50} compared to that of TRPV5(WT). Data were obtained using linear ramps from −100 to +100 mV, with a holding potential of +20 mV. (B) Histogram showing the IC_{50} of $[Ca^{2+}]_i$ on DVF current. Analysis of indicated mutants show that TRPV5(M490P) and TRPV5(M490C) has significantly higher IC_{50} compared to that of TRPV5(WT). Values are shown as mean ± SEM. $*P < 0.05$, comparison with TRPV5(WT).

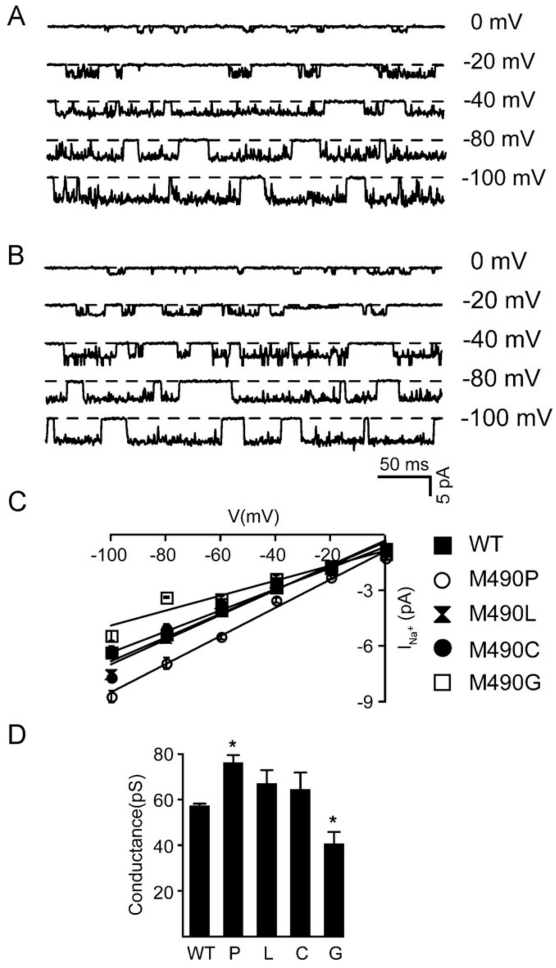

Fig. 8.

Mutating M490 to a Proline increased single channel conductance. (A and B) Current traces from a cell-attached patch of TRPV5(WT) and TRPV5(M490P) in response to hyperpolarizing steps from −100 mV to 0 mV in 20 mV increments. Non-transfected HEK293 cells did not show similar single channel activities. (C) *I/V* relationship obtained from the single channel data of respective mutants depicted in the panel. (D) Histogram showing single channel conductance of TRPV5(WT) and respective mutant channels. Single channel currents from TRPV5(M490D) in the cell attached mode were not detectable, probably due to a very low current amplitude of the mutant. Data are shown as mean ± SEM, obtained from 5 to 7 cells. **P* < 0.05, comparison with TRPV5(WT).

Table 1

The effect of TRPV5(M490P) mutation on relative permeability of monovalent cations and Ca^{2+} to Na^{+}.

	TRPV5(WT)	TRPV5(M490P)
E_{rev}		
Na^+	14.04 ± 1.41	8.38 ± 1.00
Li^+	8.21 ± 1.59	1.48 ± 0.93
K^+	−0.57 ± 1.84	−7.95 ± 1.31
Rb^+	−4.27 ± 2.11	−11.30 ± 1.36
Cs^+	−5.61 ± 2.04	−12.80 ± 1.44
$NMDG^+$	−52.25 ± 4.85	−44.50 ± 5.39
Ca^{2+}max	41.08 ± 5.30	25.32 ± 3.88
Ca^{2+}min	−2.65 ± 3.48	13.39 ± 1.49
P_{X+}/P_{Na+}		
Li^+	0.80 ± 0.01	0.77 ± 0.01
K^+	0.57 ± 0.01	0.53 ± 0.02
Rb^+	0.50 ± 0.03	0.47 ± 0.02
Cs^+	0.47 ± 0.03	0.45 ± 0.02
$NMDG^+$	0.07 ± 0.01	0.16 ± 0.03
P_{Ca2+}/P_{Na+}		
Ca^{2+}_{max}	113.63 ± 47.22	24.52 ± 6.04
Ca^{2+}_{min}	4.30 ± 1.27	9.10 ± 0.85
Permeability sequence	$Na^+ > Li^+ > K^+ > Rb^+ > Cs^+$	$Na^+ > Li^+ > K^+ > Rb^+ > Cs^+$
Eisenman sequence	X	X

Data are shown as mean ± SEM.